REVIEW ARTICLE
doi: 10.2306/scienceasia1513-1874.2024.029

*ScienceAsia* 50 (1): 2024: ID 2024029: **1–11**

# Theoretical calculations for modeling carbon-carbon coupling reactions on copper surface: A comprehensive review

**Klichchupong Dabsamut, Kaito Takahashi***

Institute of Atomic and Molecular Sciences, Academia Sinica, No 1, Sec 4 Roosevelt Road, Taipei 10617 Taiwan

*Corresponding author, e-mail: kt@gate.sinica.edu.tw

*Received 25 Jan 2024, Accepted 25 Feb 2024*
*Available online 10 Mar 2024*

**ABSTRACT**: Converting $CO_2$ to valuable chemicals at ambient conditions has been a topic of great interest due to the large impact of $CO_2$ on global warming. Electrochemical $CO_2$ reduction reaction (CRR) has been considered an effective method to produce valuable products at ambient conditions. Recently, there has been a special focus toward C2+ products, such as $C_2H_4$, $C_2H_5OH$, or $C_3H_7OH$, which have higher energy densities and large applications in chemical industries. Copper surfaces, especially those derived from its oxidized variant, have been experimentally found to be selective for C2 products. In this mini-review, we delve into the recent advances in theoretical calculations for molecular level understanding of the key step of C2 production, the carbon-carbon (CC) coupling reaction. We discuss various methods that have been developed to model the complex electrode surface, including the change in electrode potential, the effect of electrolytes, and intertwining reaction intermediates. We also present a detailed evaluation concerning the errors induced by the different approximations and the importance of solvation and asymmetric reaction environments for CC coupling. Lastly, we summarize with an outlook and possible future research direction, such as simulating experimental observables for vibrational and X-ray absorption spectra at electrode working conditions.

**KEYWORDS**: $CO_2$ reduction reaction, carbon-carbon bond formation, copper surface, density functional theory, modeling electric double layer

## INTRODUCTION

Due to the increase in the concentration of $CO_2$ in the atmosphere initiated by human activities, we are presently facing a global warming crisis. Electrochemical $CO_2$ reduction reaction (CRR) is one of the techniques for utilizing this $CO_2$ to realize a sustainable energy conversion and a carbon-neutral society [1–5]. There have been many important advances in increasing the selectivity and Faradic efficiency for 2 $e^-$ reduced products, CO and HCOOH. On the other hand, we are still searching for suitable catalysts for producing C2+ products, such as $C_2H_4$, $C_2H_5OH$, or $C_3H_7OH$, which have higher energy densities and large applications in chemical industries [6]. From the early works of Hori and coworkers [7–9], Cu surface has been studied extensively [10–14], and studies have reported that 17 different products, including the C2+ ones, can be produced from Cu foil [15–19]. However, the selective production of C2+ products has been hampered due to the slow kinetics and uncertainties in the reaction mechanism. Various experimental techniques, such as IR absorption spectra, Raman scattering spectra, and X-ray absorption spectra, have been developed to elucidate the molecular level reaction mechanism and clarify the local environment of an electrode surface. Furthermore, various facets show different reactivity, and experimentalists have found that Cu (100) is more favorable for C2 production compared to Cu (111) [20]. In addition, recent experimental studies have focused on the effect of Cu surfaces derived from oxidized copper [10]. These oxidized copper derived surfaces have shown favorable C2+ production compared to pure Cu surfaces.

Following the seminal paper by Norskov et al [21], which introduced the concept of computational hydrogen electrode (CHE), theoretical calculations based on density functional theory (DFT) methods have become a key tool to analyze electrochemical reactions on interfaces at the molecular level. Peterson et al [22] have utilized this CHE approach with DFT calculations to provide an understanding of the electroreduction of $CO_2$ to hydrocarbon fuels on the Cu (211) surface. Considering that there are various reviews on CRR, here we focus on theoretical calculations toward understanding the reaction mechanism for $C_2H_4$ and $C_2H_5OH$ production. Many previous studies [12, 23–26] have shown that the carbon-carbon (CC) coupling reaction [27–31] is the bottleneck [32–35] for the slow reactivity of C2 products [36–40]. In this review, we will focus on utilizing theoretical calculations to rationalize reaction mechanisms and further provide hints for designing better catalysts. The manuscript is organized in the following manner. In the next section, we will discuss various theoretical methods that are presently applied to study CRR, focusing on CC coupling. In addition to various quantum chemical methods, we will also discuss techniques that are utilized to include the effect of electrode potential as well as electrolytes, i.e., the electric double layer. Then, in the following section, we will summarize various molecular level findings, such as transition state energies for the CC coupling step and how it is

affected by electrode potential and electrolytes. In this section, we will also discuss the geometries of the CC coupling intermediates and summarize some key parameters that help rationalize the favorable CC coupling barriers on oxide derived copper surfaces. In the final section, we will summarize with some outlook for future direction for theoretical calculation in understanding CC coupling reactions for CRR.

## THEORETICAL CALCULATION METHODS

Before starting the discussion of various theoretical methods, it is important to first lay out the present knowledge we have about C2 product production on the Cu surface, which is given in Fig. 1. Chemisorption of $CO_2$ to Cu surface and electron transfer results in an activated bent $*CO_2$ (We will use * to symbolize the adsorbed state). The protonation of the oxygen coupled with an electron transfer from the electrode gives *COOH. Further proton coupled electron transfer to the oxygen atom produces $H_2O$ molecule and *CO. Then the concentration of surface *CO can increase where two neighboring *CO could couple to form *OC–CO, resulting in

$$2{}^*\mathrm{CO} \rightarrow {}^*\mathrm{OC{-}CO}. \quad \text{(R1)}$$

On the other hand, another proton coupled electron transfer can occur to form *CHO or *COH. Then, these reduced products may couple with a *CO to give

$${}^*\mathrm{CO} + {}^*\mathrm{CHO} \rightarrow {}^*\mathrm{OC{-}CHO}, \quad \text{(R2)}$$
$${}^*\mathrm{CO} + {}^*\mathrm{COH} \rightarrow {}^*\mathrm{OC{-}COH}. \quad \text{(R3)}$$

If the concentration of the reduced products increases, we can also have

$${}^*\mathrm{CHO} + {}^*\mathrm{CHO} \rightarrow {}^*\mathrm{OHC{-}CHO}, \quad \text{(R4)}$$
$${}^*\mathrm{COH} + {}^*\mathrm{COH} \rightarrow {}^*\mathrm{HOC{-}COH}, \quad \text{(R5)}$$
$${}^*\mathrm{COH} + {}^*\mathrm{CHO} \rightarrow {}^*\mathrm{HOC{-}CHO}. \quad \text{(R6)}$$

Further reduced products such as $*CH_x$, where $x = 1$, 2, or 3, may also couple with the surface adsorbed *CO giving:

$${}^*\mathrm{CO} + {}^*\mathrm{CH}_x \rightarrow {}^*\mathrm{OC{-}CH}_x. \quad \text{(R7)}$$

In the following section, we will discuss the present knowledge concerning the different CC coupling reactions mentioned above based on theoretical calculations of Cu surfaces. We focus on reaction R1 since many previous calculations have mentioned that this CC coupling step is critical on the Cu surface.

### DFT Calculations

The DFT method with periodic boundary conditions has been the main working horse for calculating bulk transition metal interfaces. One can calculate complex electronic states of reactive processes on the Cu surface utilizing various computational packages. In many cases, a slab model using four to five layers of Cu is utilized to model the direction perpendicular to the surface. We also include a 10 to 15 Å vacuum or electrolyte layer to model an interface. Since one will model the coupling reaction of *CO+*CO, *CO+*COH, *CO+*CHO, or CO+$CH_x$, a unit cell consisting of $3 \times 3$ to $5 \times 5$ is used for the direction in the plane of the surface. In many early studies, the calculations were performed in the vacuum and used the Perdew-Burke-Ezenhoff functional [41] with Grimme's dispersion corrections [42] (PBE-D3). The effect of the electrode potential is included as additional free energy correction following the CHE model of Norskov et al [21] (see below for progress in methods for including the effect of the electrode potential). The kinetics of a reaction is determined by the transition state connecting the reactant and products, and the value of the barrier energy becomes key. In the literature, this barrier energy is referred to as the activation energy or the transition state energy and is usually obtained using the nudged elastic band method by connecting reactant and product geometries [43].

### Embedding methods

To go beyond the DFT level of theory, some researchers use embedding methods, which allow the use of high-level quantum chemistry calculation for a local cluster cut out of the interface reaction system, while lower-level methods model the remaining Cu surface. In the embedded correlated wavefunction theory method, Carter and coworkers utilized $Cu_{10}$ and $Cu_{12}$ cluster models to study the reactions R1 to R5 using the multireference complete active space self-consistent field method with perturbative corrections (CASPT2) [38]. The remaining Cu atoms in the five layer $5 \times 5$ surface slab model of Cu (111) surface were modeled by periodic boundary PBE-D3 to obtain the embedded CASPT2 (emb-CASPT2) energies. In a similar concept, Xu and coworkers used the "extended our own n-layered integrated molecular orbital method" (XO) [44]. Here, the double hybrid XYG3 functional method was used to model a $Cu_{31}$ cluster, while the PBE-D3 method with periodic boundary was used for the remaining Cu (111) surface. In both cases, they saw differences of half an eV compared to the pure PBE-D3 calculations for the energies of CC coupling reactions. For example, Xu and coworkers found that the reaction energy for R2 and R3 was 0.63 and 0.86 eV by the XO XYG3:PBE-D3 method while it was 0.08 and 0.22 eV by PBE-D3. Furthermore, the barrier energy for reaction R2 and R3 was calculated to be 0.86 and 0.74 eV by PBE-D3, but the emb-CASPT2 method gave 1.23 and 1.55 eV. These studies highlight that the barrier energy and the heat of reaction may be underestimated by PBE-D3 calculations.

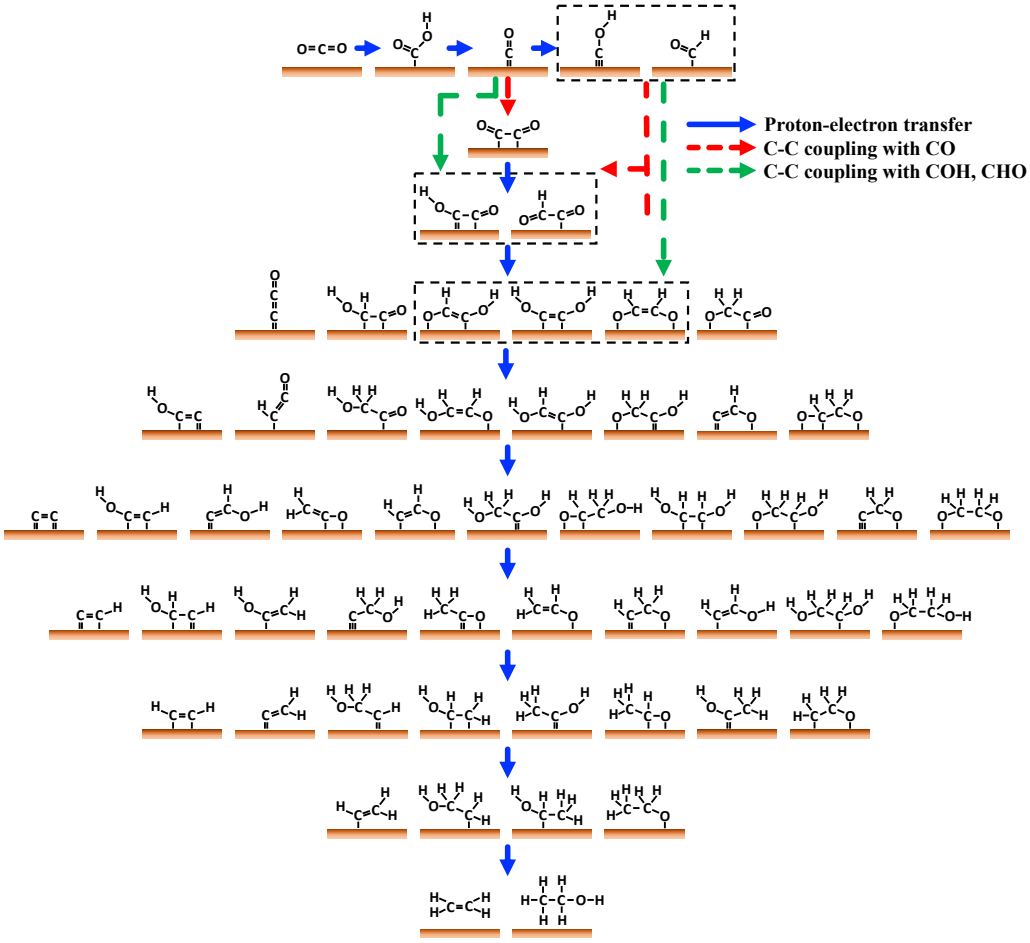


**Fig. 1** Schematic $CO_2$ reduction reaction process for producing $C_2H_5OH$ and $C_2H_4$. Proton coupled electron transfer is given with solid blue arrows, while CC coupling is given with dashed arrows.

### Modeling the electrolytes

In many cases, the electrocatalytic CRR is performed in the aqueous phase at various acidic or basic conditions, so it is also important to consider the effect of the electrolyte, water molecules, and ions such as $Li^+$ or $Cs^+$. On the other hand, the use of CHE approximation allows one to connect the free energy of $H^+(aq) + e^-$ to be equal to that of half of $H_2$ gas, and one can use the theoretical value in the gas phase to model the thermodynamics of complex reduction reactions under the assumption of proton coupled electron transfer. As mentioned above, electrocatalytic CRR usually occurs in the aqueous phase, and recent studies incorporate these effects of water molecules explicitly and implicitly [25, 36]. The water molecules are placed onto the surface and calculated using DFT methods in the first method. Initially, only a few active water molecules around the reaction center were considered, but recently, three to five layers totaling 30 to 40 water molecules have been incorporated in the DFT calculations of slab models [29]. Since increased water molecules mean various hydrogen bonding conformations above the surface, we must consider sampling various hydrogen bonding geometries. As discussed by Chan and coworkers, this sampling can induce nearly 0.5 eV variation in energy [45].

On the other hand, for implicit modeling, one models the aqueous condition as an effective polarizable continuum media with parameter $\varepsilon$; thus, we can ignore sampling [46–48]. However, this method ignores local hydrogen bonding interactions contributing to the solvation energy of the intermediates on the Cu surface. We note several *ad hoc* energy corrections for the solvation energy have also been reported based on the number of hydrogen atoms on the adsorbate [22, 48].

### Constant potential models

In the CHE, the free energy, G, of the reaction for a proton coupled electron transfer step, such as

*CO+$H^+$(aq)+$e^-$→*CHO can be modeled as $G_{*CHO} - \left(G_{*CO} + \frac{1}{2}G_{H_2} - eU\right)$, where $U$ is the electrode potential with respect to the standard hydrogen electrode (SHE), and e is the charge of an electron [21]. For CC coupling reactions, since there is no proton coupled electron transfer, the effect of the potential is ignored if we use the CHE. However, as one may guess, changing the electrode potential will cause a change in charge on the Cu surface [49]. Therefore, ignoring this effect may not be a good approximation, especially for CRR, which occurs at negative potentials $-0.4 \sim -1.1$ V vs SHE. In many DFT simulations, we assume the total number of electrons is constant (constant charge). We usually use neutral unit cells to remove artificial interaction among the periodic images. However, to consider constant electrode potential, we need to allow fluctuations in the number of electrons due to the coupling with the Cu electrode. In CHE, the effect of the electrode potential, U, is added as an external energy correction to the energies calculated by DFT at a constant number of electrons. However, this does not include the charging effect of the electrode surface due to the variation in the electrode potential. Various grand canonical ensemble DFT methods have been developed to model such electrode potential dependence. In these methods, the number of electrons is modulated in the DFT calculation, and the theoretical work function of the Cu surface is used to define the electrode potential of the calculated surface [47]. Both explicit and implicit forms of solvation models are applied in these simulations [25, 36]. We note that in the simulations, a continuous background charge compensates for the extra charge induced by adding or subtracting the fractional number of electrons. Recently, several different approximations have been developed to model the effect of the electrode potential. One is based on calculating the charge buildup at the interface layer and extrapolating between the initial and final geometries [50]. Otani and Sugino developed an efficient method to screen the excess surface charge by imposing proper boundary conditions [51]. Another method uses a plate type electric field and performs the calculation under constant charge conditions [52]. Including neutral Li or Na atoms into the explicit water layer can also result in an electron transfer to the Cu surface and be used to model the negatively charged surface [53]. In Fig. 2, we have placed a schematic representation of the various methods mentioned above.

As seen in this section, various methods allow one to include the effect of electrode potential and electrolytes. We think it will be important to use the same level of electronic structure calculation and evaluate the consistencies among various methods.

## MOLECULAR LEVEL FINDINGS

In the following, we focus on a few insights obtained from the theoretical DFT calculations. As mentioned above, PBE-D3 may have errors of $\sim 0.5$ eV, and solvation sampling can also add in $\sim 0.5$ eV variations in energy. So, the key point will be discussing the general trends.

### Effect of hydration toward CC coupling barriers

In Fig. 3, we present the calculated reactant, product, and barrier geometries for reaction R1 on various Cu surfaces. We used the projector-augmented wave method implemented in the Vienna Ab initio Simulation Package [54, 55] with PBE-D3 [42, 56]. We used a kinetic energy cutoff of 500 eV for the plane-wave expansion. We used Monkhorst-Pack $3 \times 3 \times 1$ k-point mesh for the Brillouin zone integration. We set our convergence criteria as total energy difference less than $10^{-5}$ eV and Hellmann-Feynman forces less than 0.02 eV/Å across all optimizations. To mitigate interaction between the Cu surface and its periodic image, we introduced a vacuum layer of 15 Å along the direction perpendicular to the surface.

These calculations show that for Cu (111), (110), and (100), the CC coupling product OCCO is bound to the surface with carbon and oxygen atoms (CO bound). On the other hand, for the high index (211) and (511) surfaces, we obtain OCCO in which two carbon atoms are bound (CC bound) to the Cu surface. As discussed by Santatiwongchai et al, who used PBE-D3 DFT with five layers of implicit water on Cu (100), the hydration causes the reaction free energy to change greatly for reaction R1, 2*CO→*OC—CO. In the vacuum, it is exothermic by 1.1 eV, while it becomes nearly isoenergetic if we consider the hydration [29]. Furthermore, their calculations show that the OCCO product takes the CO bound form in vacuum calculations, but with implicit water layers, it takes the CC bound form. Montoya et al also observed that the CC bound form is stabilized on both Cu (111) and (100) surfaces when calculated using PBE-D3 with a monolayer of water [32]. They also showed that the local electric field initiated by the solvating water molecule can help stabilize *OCCO adsorption compared to 2*CO.

### Electrode potential dependence of CC coupling barriers

To study the 2*CO→*OC—CO reaction on the Cu (100) surface, Head-Gordon and coworkers used PBE-D3 with implicit solvation with electrode potential correction using grand canonical DFT [25]. In their calculation, they changed the electrode potential from $U = 0$ and $-1.0$ V versus the relative hydrogen electrode at pH $= 7$ and found that the barrier for CC coupling increases slightly from 0.6 eV to 0.7 eV. On the other hand, the heat of reaction decreased from 0.5 eV to 0.2 eV. So, the effect of a negatively charged surface can greatly affect the heat of reaction for 2*CO→*OC—CO by stabilizing the product. Tsai and coworkers used PBE-D3 to model the same reaction on

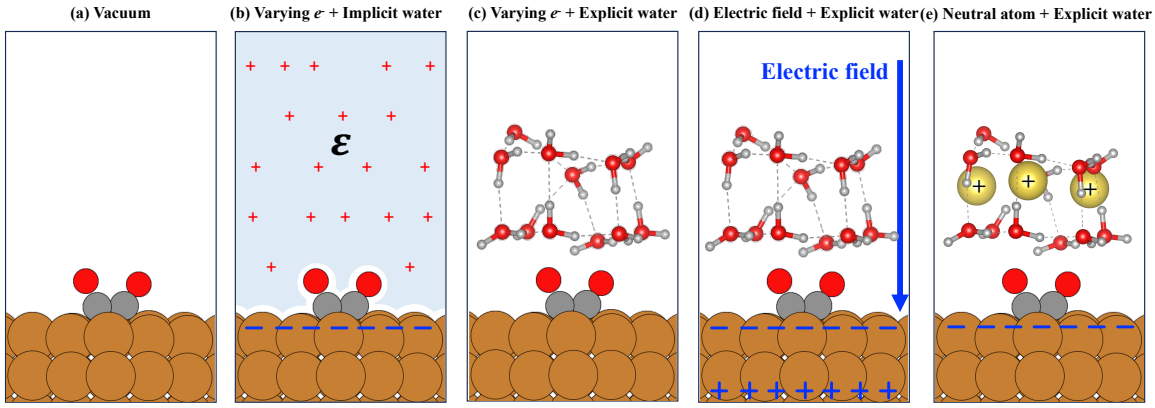


**Fig. 2** Schematic models used to calculate copper electrolyte interfaces, including the effect of electrode potential. (a) vacuum, (b) varying the number of electrons and using implicit water [25], (c) varying the number of electrons and using explicit water [36], (d) applying an electric field with explicit water [52], (e) adding in atoms and explicit water [53].

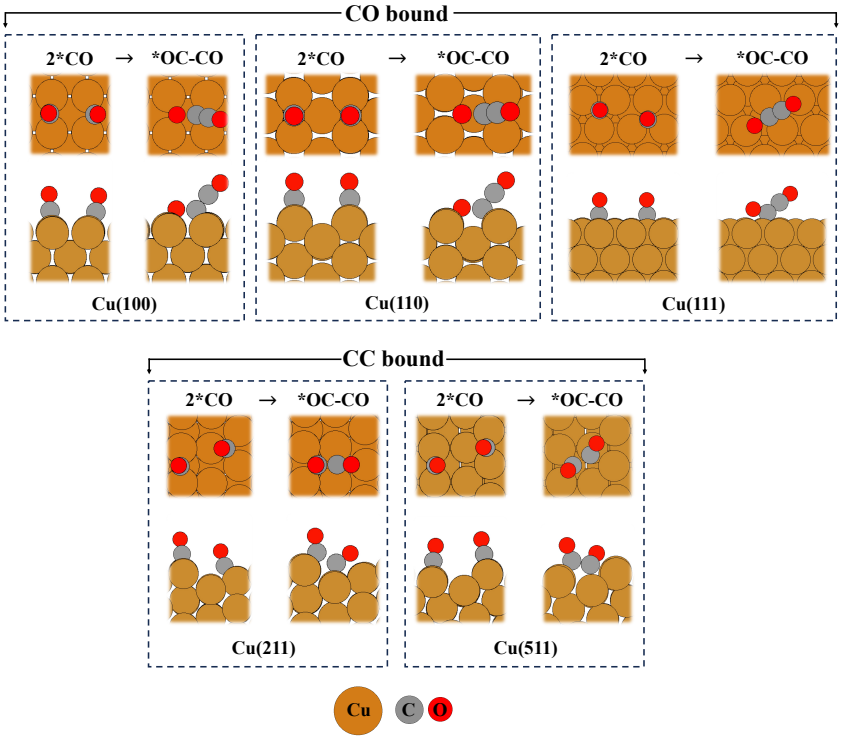


**Fig. 3** Schematic geometry for 2*CO→*OC—CO, reaction R1, calculated for Cu surface on various facets in vacuum.

the Cu (111) surface, including three to four layers of water molecules and a plate type electric field [52]. They also found a slightly increasing barrier energy and a great decrease in the heat of reaction in going from positive to negative electrode potential U. Furthermore, in their analysis, they found that at 2*CO, the Cu surface donates ∼ 1 electron to the adsorbates, on the other hand, after the CC coupling this increases to ∼ 1.6 electrons for *OCCO configuration. This signifies that the product OCCO is more negatively charged, and hydrogen bonding of the water also stabilizes this excess charge by shortening the average CO…$H_2O$ distance by 0.3 Å. The large negative potential results in favorable electron transfer to the *OCCO, and stabilization of this CC coupling product can be further enhanced by a larger hydration energy of the more negatively charged *OCCO.

Considering that this effect of electrode poten-

tial and solvating water molecules greatly affects the charge transfer between the Cu surface and the adsorbates, we also have to be careful about the accuracy of the charge transfer. Carter and coworkers have compared the difference in binding energies of CC coupling intermediates using PBE-D3 and emb-CASPT2 [38]. They found that intermediates with large energy differences between the two methods have large differences in the adsorbate charge change. Therefore, they concluded that inaccurate charge transfer from the metal surface is one sign when evaluating the accuracies in the energies. On the other hand, charge transfer is very sensitive to the work function of the surface, and in the embedding methods, one may need to check the convergence with respect to the embedded cluster size.

### Reactivity on the oxidized copper surface

Experimental studies by Kanan and coworkers showed enhanced production of C2 products on electrodes derived from oxidized copper produced by annealing copper foil in air [10]. Considering that CRR occurs at negative electrode potentials (−0.4 to −1.1 V SHE), the Cu(+1) oxidation state is expected to be reduced at experimental electrocatalytic conditions. Detailed experimental studies have found that the number of grain boundaries can be related to the activity of producing C2 products. Goddard and coworkers have performed calculations on pristine Cu (111) surface, fully oxidized $Cu_2O$ surface, and Cu embedded $Cu_2O$ surface; see schematic geometries in Fig. 4 [35]. They used PBE with a mixed implicit explicit solvation model coupled with grand canonical DFT and showed that at $U = -0.9$ V vs SHE, the barrier for reaction R1, 2*CO→*OC−CO, was 1.1, 3.2, and 0.71 eV on the pristine Cu, full oxidized $Cu_2O$, and Cu embedded $Cu_2O$ surface, respectively. Importantly, they showed that the reduced barrier energy in the Cu embedded $Cu_2O$ surface was due to the different atomic charges on the two *CO on the surface. The *CO on the $Cu_2O$ had a slightly positively charged carbon atom, while that on embedded Cu had a slightly negatively charged carbon atom (see bottom panel of Fig. 4). This favorable electrostatic interaction among the 2*CO on the Cu embedded $Cu_2O$ surface results in lower barriers than pristine Cu or $Cu_2O$ surfaces. Indeed, if the CC coupling reaction was performed only on the Cu surface that is embedded in the $Cu_2O$, the barrier was similar to that obtained from the pristine Cu surface. This shows that grain boundaries are important features for CC coupling, and experimental studies have shown a correlation between the amount of grain boundary and $C_2H_4$ faradic efficiency. In conclusion, an asymmetric environment is vital in promoting CC coupling.

Wu and coworkers evaluated the optimum Cu-Cu distance for favorable CC coupling barriers in generating $C_2H_4$ using PBE functional on $Cu_2O$ (100) surface [57]. Interestingly, they found that if the two active Cu are 1.5 Å apart, the hydrogen evolution reaction producing $H_2$ is active, while if it is 3.5 Å apart, formic acid production is favored. According to their study, favorable ethylene production was predicted if the Cu distance was 2.5 Å apart. Norskov and coworkers also studied the effect of strain on the Cu (100), (111), and (211) surfaces and found tensile strain can cause the CC coupling barrier to decrease [24]. This shows constraining the active site distance is one way to reduce the CC coupling barrier, but we have

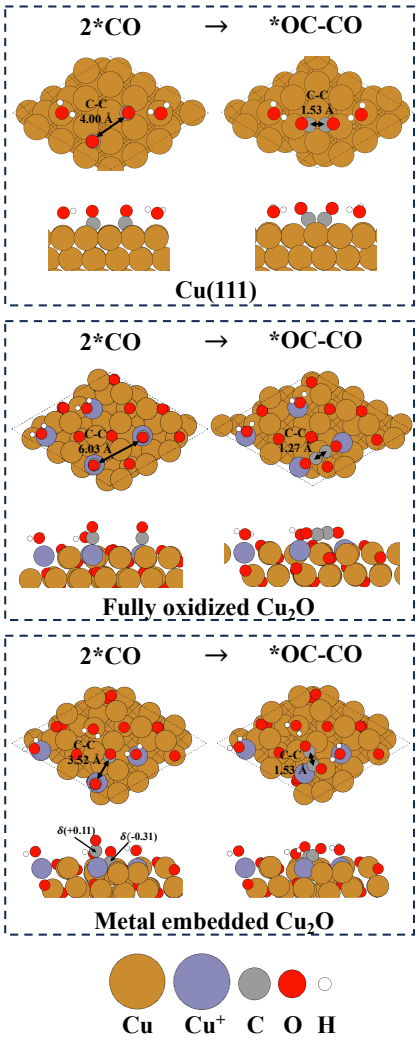


**Fig. 4** The pristine Cu (111) surface, fully oxidized $Cu_2O$ surface, and metal embedded $Cu_2O$ surface. Orange, blue, gray, red, and white balls stand for Cu, embedded Cu, carbon, oxygen, and hydrogen atoms. We obtained the charge on the CO of the metal embedded $Cu_2O$ surface from Xiao et al [35].

to remember that in electrode working conditions, surface reconstructions may occur, and keeping the ideal distance at experimental conditions may not be as easy as in a computational perspective.

## CONCLUSION AND OUTLOOK

As we have summarized above, theoretical calculations have helped rationalize various experimental findings on CC coupling on the Cu surface, and researchers are developing various models to describe the complex electric double layer of the electrode-electrolyte interface. We have collected CC coupling barrier energies from recent theoretical calculations on Cu surface in Table 1, following the format used by Nitopi et al [19]. As discussed in many experimental reviews, developing *in situ* surface sensitive techniques that detect important reaction intermediates at electrode operating conditions will become key for understanding the reaction mechanism and finding suitable catalysts for CRR to form C2+ products selectively. Following this lead for new experimental instrumentation, theoretical studies will also need to develop new methodologies to simulate IR absorption or Raman scattering spectra under operating conditions [58]. Koper and coworkers have reported the vibrational spectra of C2+ intermediates at experimental electrode conditions with assignments based on frequencies calculated by DFT calculations [12]. Ab initio molecular dynamics simulation at a constant charge DFT level was recently used to simulate vibrational spectra of CC coupling reaction intermediates to help assign the experimental spectra on oxide derived copper surfaces [59]. So combining the various electrolyte models as well as electrode potential calculation methods to quantitatively determine the vibrational spectra change during the electrode working condition will be one important direction for the future [60].

In addition, surface reconstruction at operating electrode CRR conditions is one of the reasons for the decrease in activity for oxide derived copper surfaces. Recent studies have shown that the catalyst activity toward producing ethylene of these Cu surfaces can be elongated by alternating "on" and "off" operating regimes [61]. During the "on" time, the catalyst is reduced at very negative electrode potentials. It is oxidized during the "off" time due to the interaction with available oxygen in the atmosphere. Furthermore, pulsing the electrode potential has also been shown to allow efficient steering of ethanol on Cu surfaces [62]. Another recent study has mentioned that co-electrolysis of $CO_2$ with $O_2$ can modulate the Cu surface and promote the formation of C2 products [63]. Therefore, detailed calculations helping to understand the surface reconstruction at working electrode conditions and its recovery will also be an important direction for producing stable catalyst surfaces for CRR [64].

Thirdly, several studies have mentioned the importance of cations, such as $Cs^+$, in promoting the CC coupling to produce ethanol. Detailed theoretical models to evaluate the effect of these cations and anions near the electrode interface will likely shed light on the complex reactions occurring on electrocatalytic CRR. Since these ions can be in the electrolyte near the adsorbates, directly adsorb on or desorb from the surface (depending on the electrode potential), and modulate the local pH around the electrode, one will need detailed modeling of the dynamics of these ions involving adsorption, desorption, and mass transport. We believe that detailed modeling of the electrode interface $C_2H_5OHs$ complex local reaction environment will further enhance our understanding of electrocatalytic reactions [49].

Lastly, so-called single atom catalysts (SACs), which are based on localized atomic active sites for reactions, have attracted attention due to their favorable utilization of metal atoms [65, 66]. Similarly, dual-atom catalysts (DACs) have also been studied, and some show promising results for CC coupling reactions [67–70] Compared to traditional copper-based catalysts, these SACs and DACs offer enhanced selectivity and efficiency, spotlighting the potential for broader material exploration. Furthermore, utilizing various substrate materials and defect engineering, one can modulate the electronic state of the active metal site which can provide flexibility and fine tuning for favorable CC coupling. We believe computational studies can help rationalize the effect of the substrate on the local electronic structure of the metal active site. Some studies have even mentioned that non-metal carbon based surfaces can also promote CC coupling [71, 72]. All in all, copper remains the most well-studied metal surface for C2 production for CRR, but extension toward other materials is another direction for computational studies to explore. Furthermore, for these carbon based materials, the surface stability has not been studied in detail compared to metal surfaces, and computational studies may help provide molecular level changes in bonding geometries at electrode working conditions.

*Acknowledgements*: K.T. thanks the funding support from the National Science and Technology Council (NSTC 111-2113-M-001-049 and 112-2113-M-001-037) and Academia Sinica.

## REFERENCES

1. Park JH, Yang J, Kim D, Gim H, Choi WY, Lee JW (2022) Review of recent technologies for transforming carbon dioxide to carbon materials. *Chem Eng J* **427**, 130980.
2. Xu S, Carter EA (2019) Theoretical insights into heterogeneous (photo)electrochemical $CO_2$ reduction. *Chem Rev* **119**, 6631–6669.
3. Álvarez A, Borges M, Corral-Pérez JJ, Olcina JG, Hu L, Cornu D, Huang R, Stoian D, et al (2017) $CO_2$ activation over catalytic surfaces. *ChemPhysChem* **18**, 3135–3141.

**Table 1** Previously calculated C—C coupling barrier in different methods from the literature.

| Water molecules | TS search method | Potential dependence | C—C coupling reaction | Facet | pH | Potential (vs. RHE) | Barrier (eV) | Ref. |
|---|---|---|---|---|---|---|---|---|
| 0 | NEB | – | OC–CO | (100) | – | – | 1.26 | [73] |
| 0 | – | Bader charge of adsorbates | OC–CO | (100) | – | – | 1.19 | [23] |
| 0–2 | Dimer | Implicit solvent | OC–CO<br>OC–CHO | (100) | 7 | 0 | 0.53<br>0.63 | [25] |
| 1 to 2 | H shuttling | Implicit solvent | OC–CO | (111) | 1<br>7<br>12 | 0 | 1.15<br>1.14<br>1.14 | [74] |
| 48 | Metadynamics | Charge extrapolation | OC–CO | (100) | 7 | −0.59 | 0.69 | [36] |
| 0 | Dimer | Implicit solvent | OC–CHO | (100)<br>(511) | – | – | 0.43<br>0.47 | [75] |
| 1<br>2 | H shuttling | H shuttling | OC–CO | (100) | – | – | 1.22<br>1.06 | [76] |
| 1 | | | OC–CHO<br>OC–CO | (100)<br>(111) | | | 0.77<br>1.7 | |
| 5 (1 layer) | NEB | Charge extrapolation | OC–CO | (100)<br>(111)<br>(211) | – | – | 0.45<br>0.72<br>0.72 | [77] |
| 2 | – | – | OC–CO | (100)<br>(111)<br>(100/100)<br>(111/111)<br>(100/111) | – | – | 0.44<br>0.95<br>0.40<br>0.76<br>0.29 | [78] |
| 34 (3 layers) | Dimer | – | OC–CO<br>OC–CHO<br>OC–COH | (100) | – | – | 0.49<br>0.91<br>0.68 | [29] |
| 4 | Eigen complex | Implicit solvent | OC–CO<br>OC–CHO<br>HC–CH<br>HC–CHO<br>HC–$CH_2$ | (110) | 6.8 | −1 | 0.61<br>0.90<br>0.47<br>0.62<br>0.52 | [28] |
| 0 | NEB | Implicit solvent | OC-CHO | (100)<br>(110)<br>(111) | – | – | 0.55<br>0.75<br>0.81 | [79] |
| 0 | NEB | ECW | OC–CO<br>OC–COH | (111) | – | – | 0.59<br>1.55 | [38] |
| | | | OC–CHO | | | | 1.23 | |
| 1 | | | | | | | 1.07 | |
| 0 | NEB | – | OC–CO<br>OC–COH | (711) | – | – | 1.69<br>0.35 | [80] |
| 0<br>44 (6 layers) | NEB | Plate-type efields | OC–CO | (111) | – | – | 2.25<br>1.12 | [52] |
| | | | | | | | 0.95 | |
| 22 (3 layers) | | | | | 7 | 1.77 | 0.95 | |
| | | | | | 7 | −0.57 | 0.96 | |


4. Kumar B, Brian JP, Atla V, Kumari S, Bertram KA, White RT, Spurgeon JM (2016) New trends in the development of heterogeneous catalysts for electrochemical $CO_2$ reduction. *Catal Today* **270**, 19–30.
5. Kibria MG, Edwards JP, Gabardo CM, Dinh C-T, Seifitokaldani A, Sinton D, Sargent EH (2019) Electrochemical $CO_2$ reduction into chemical feedstocks: From mechanistic electrocatalysis models to system design. *Adv Mater* **31**, 1807166.
6. Yan T, Chen X, Kumari L, Lin J, Li M, Fan Q, Chi H, Meyer TJ, et al (2023) Multiscale CO(2) electrocatalysis to C(2+) products: Reaction mechanisms, catalyst design, and device fabrication. *Chem Rev* **123**, 10530–10583.
7. Hori Y, Kikuchi K, Suzuki S (1985) Production of CO and $CH_4$ in electrochemical reduction of $CO_2$ at metal electrodes in aqueous hydrogencarbonate solution. *Chem*

*Lett* **14**, 1695–1698.
8. Hori Y, Wakebe H, Tsukamoto T, Koga O (1994) Electrocatalytic process of CO selectivity in electrochemical reduction of $CO_2$ at metal electrodes in aqueous media. *Electrochim Acta* **39**, 1833–1839.
9. Hori Y, Takahashi I, Koga O, Hoshi N (2003) Electrochemical reduction of carbon dioxide at various series of copper single crystal electrodes. *J Mol Catal A Chem* **199**, 39–47.
10. Li CW, Ciston J, Kanan MW (2014) Electroreduction of carbon monoxide to liquid fuel on oxide-derived nanocrystalline copper. *Nature* **508**, 504–507.
11. Handoko AD, Chan KW, Yeo BS (2017) $CH_3$ mediated pathway for the electroreduction of $CO_2$ to ethane and ethanol on thick oxide-derived copper catalysts at low overpotentials. *ACS Energy Lett* **2**, 2103–2109.
12. Pérez-Gallent E, Figueiredo MC, Calle-Vallejo F, Koper MTM (2017) Spectroscopic observation of a hydrogenated CO dimer intermediate during CO reduction on Cu (100) electrodes. *Angew Chem Int Ed* **56**, 3621–3624.
13. Wang J, Tan H-Y, Zhu Y, Chu H, Chen HM (2021) Linking the dynamic chemical state of catalysts with the product profile of electrocatalytic $CO_2$ reduction. *Angew Chem Int Ed* **60**, 17254–17267.
14. Pablo-García S, Veenstra FLP, Ting LRL, García-Muelas R, Dattila F, Martín AJ, Yeo BS, Pérez-Ramírez J, et al (2022) Mechanistic routes toward C3 products in copper-catalysed $CO_2$ electroreduction. *Catal Sci Technol* **12**, 409–417.
15. Resasco J, Chen LD, Clark E, Tsai C, Hahn C, Jaramillo TF, Chan K, Bell AT (2017) Promoter effects of alkali metal cations on the electrochemical reduction of carbon dioxide. *J Am Chem Soc* **139**, 11277–11287.
16. Pérez-Gallent E, Marcandalli G, Figueiredo MC, Calle-Vallejo F, Koper MTM (2017) Structure- and potential-dependent cation effects on CO reduction at copper single-crystal electrodes. *J Am Chem Soc* **139**, 16412–16419.
17. Bertheussen E, Verdaguer-Casadevall A, Ravasio D, Montoya JH, Trimarco DB, Roy C, Meier S, Wendland J, et al (2016) Acetaldehyde as an intermediate in the electroreduction of carbon monoxide to ethanol on oxide-derived copper. *Angew Chem Int Ed* **55**, 1450–1454.
18. Kuhl KP, Cave ER, Abram DN, Jaramillo TF (2012) New insights into the electrochemical reduction of carbon dioxide on metallic copper surfaces. *Energy Environ Sci* **5**, 7050–7059.
19. Nitopi S, Bertheussen E, Scott SB, Liu X, Engstfeld AK, Horch S, Seger B, Stephens IEL, et al (2019) Progress and perspectives of electrochemical $CO_2$ reduction on copper in aqueous electrolyte. *Chem Rev* **119**, 7610–7672.
20. Hori Y, Takahashi I, Koga O, Hoshi N (2002) Selective formation of C2 compounds from electrochemical reduction of $CO_2$ at a series of copper single crystal electrodes. *J Phys Chem B* **106**, 15–17.
21. Nørskov JK, Rossmeisl J, Logadottir a, Lindqvist L, Kitchin JR, Bligaard T, Jónsson H (2004) Origin of the overpotential for oxygen reduction at a fuel-cell cathode. *J Phys Chem B* **108**, 17886–17892.
22. Peterson AA, Abild-Pedersen F, Studt F, Rossmeisl J, Nørskov JK (2010) How copper catalyzes the electroreduction of carbon dioxide into hydrocarbon fuels. *Energy Environ Sci* **3**, 1311–1315.
23. Calle-Vallejo F, Koper MTM (2013) Theoretical considerations on the electroreduction of CO to C2 species on Cu (100) electrodes. *Angew Chem Int Ed* **52**, 7282–7285.
24. Montoya JH, Peterson AA, Nørskov JK (2013) Insights into C—C coupling in $CO_2$ electroreduction on copper electrodes. *ChemCatChem* **5**, 737–742.
25. Goodpaster JD, Bell AT, Head-Gordon M (2016) Identification of possible pathways for C—C bond formation during electrochemical reduction of $CO_2$: New theoretical insights from an improved electrochemical model. *J Phys Chem Lett* **7**, 1471–1477.
26. Garza AJ, Bell AT, Head-Gordon M (2018) Mechanism of $CO_2$ reduction at copper surfaces: pathways to C2 Products. *ACS Catal* **8**, 1490–1499.
27. Chan Y-T, Huang IS, Tsai M-K (2019) Enhancing C—C bond formation by surface strain: A computational investigation for C2 and C3 intermediate formation on strained Cu surfaces. *Phys Chem Chem Phys* **21**, 22704–22710.
28. Kuo T-C, Chou J-W, Shen M-H, Hong Z-S, Chao T-H, Lu Q, Cheng M-J (2021) First-principles study of C—C coupling pathways for $CO_2$ electrochemical reduction catalyzed by Cu (110). *J Phys Chem C* **125**, 2464–2476.
29. Santatiwongchai J, Faungnawakij K, Hirunsit P (2021) Comprehensive mechanism of $CO_2$ electroreduction toward ethylene and ethanol: The solvent effect from explicit water-Cu (100) interface models. *ACS Catal* **11**, 9688–9701.
30. Ou L, He Z (2021) Mechanism for $CO_2$ electroreduction into C2 products at the low overpotential: Theoretical insights from an improved electrode/solution interface model. *Surf Sci* **705**, 121782.
31. Xiao H, Cheng T, Goddard WA 3rd, Sundararaman R (2016) Mechanistic explanation of the pH dependence and onset potentials for hydrocarbon products from electrochemical reduction of CO on Cu (111). *J Am Chem Soc* **138**, 483–486.
32. Montoya JH, Shi C, Chan K, Nørskov JK (2015) Theoretical insights into a CO dimerization mechanism in $CO_2$ electroreduction. *J Phys Chem Lett* **6**, 2032–2037.
33. Kastlunger G, Wang L, Govindarajan N, Heenen HH, Ringe S, Jaramillo T, Hahn C, Chan K (2022) Using pH dependence to understand mechanisms in electrochemical CO reduction. *ACS Catal* **12**, 4344–4357.
34. Liu X, Schlexer P, Xiao J, Ji Y, Wang L, Sandberg RB, Tang M, Brown KS, et al (2019) pH effects on the electrochemical reduction of CO(2) towards C2 products on stepped copper. *Nat Commun* **10**, 32.
35. Xiao H, Goddard WA, Cheng T, Liu Y (2017) Cu metal embedded in oxidized matrix catalyst to promote $CO_2$ activation and CO dimerization for electrochemical reduction of $CO_2$. *Proc Natl Acad Sci USA* **114**, 6685–6688.
36. Cheng T, Xiao H, Goddard WA (2017) Full atomistic reaction mechanism with kinetics for CO reduction on Cu (100) from ab initio molecular dynamics free-energy calculations at 298 K. *Proc Natl Acad Sci USA* **114**, 1795–1800.
37. Li Y, Chan SH, Sun Q (2015) Heterogeneous catalytic conversion of $CO_2$: A comprehensive theoretical review. *Nanoscale* **7**, 8663–8683.
38. Zhao Q, Martirez JMP, Carter EA (2022) Charting C—C coupling pathways in electrochemical $CO_2$ reduction

on Cu (111) using embedded correlated wavefunction theory. *Proc Natl Acad Sci USA* **119**, e2202931119.
39. Kong X, Zhao J, Ke J, Wang C, Li S, Si R, Liu B, Zeng J, et al (2022) Understanding the effect of *CO coverage on C—C coupling toward $CO_2$ electroreduction. *Nano Lett* **22**, 3801–3808.
40. Zhi X, Jiao Y, Zheng Y, Qiao S-Z (2021) Key to C2 production: selective C—C coupling for electrochemical $CO_2$ reduction on copper alloy surfaces. *ChemComm* **57**, 9526–9529.
41. Perdew J, Burke K, Ernzerhof M (1996) Generalized gradient approximation made simple. *Phys Rev Lett* **77**, 3865–3868.
42. Grimme S, Antony J, Ehrlich S, Krieg H (2010) A consistent and accurate ab initio parametrization of density functional dispersion correction (DFT-D) for the 94 elements H-Pu. *J Chem Phys* **132**, 154104.
43. Henkelman G, Uberuaga BP, Jónsson H (2000) A climbing image nudged elastic band method for finding saddle points and minimum energy paths. *J Chem Phys* **113**, 9901–9904.
44. Chen Z, Liu Z, Xu X (2023) Accurate descriptions of molecule-surface interactions in electrocatalytic $CO_2$ reduction on the copper surfaces. *Nat Commun* **14**, 936.
45. Ludwig T, Gauthier JA, Brown KS, Ringe S, Nørskov JK, Chan K (2019) Solvent–Adsorbate interactions and adsorbate-specific solvent structure in carbon dioxide reduction on a stepped Cu surface. *J Phys Chem C* **123**, 5999–6009.
46. Fishman M, Zhuang HL, Mathew K, Dirschka W, Hennig RG (2013) Accuracy of exchange-correlation functionals and effect of solvation on the surface energy of copper. *Phys Rev B* **87**, 245402.
47. Mathew K, Sundararaman R, Letchworth-Weaver K, Arias TA, Hennig RG (2014) Implicit solvation model for density-functional study of nanocrystal surfaces and reaction pathways. *J Chem Phys* **140**, 084106.
48. Heenen HH, Gauthier JA, Kristoffersen HH, Ludwig T, Chan K (2020) Solvation at metal/water interfaces: An ab initio molecular dynamics benchmark of common computational approaches. *J Chem Phys* **152**, 144703.
49. Li P, Jiao Y, Huang J, Chen S (2023) Electric double layer effects in electrocatalysis: Insights from ab initio simulation and hierarchical continuum modeling. *JACS Au* **3**, 2640–2659
50. Chan K, Nørskov JK (2015) Electrochemical barriers made simple. *J Phys Chem Lett* **6**, 2663–2668.
51. Otani M, Sugino O (2006) First-principles calculations of charged surfaces and interfaces: A plane-wave nonrepeated slab approach. *Phys Rev B* **73**, 115407.
52. Liao C-C, Tsai T-H, Chang C-C, Tsai M-K (2023) The use of plate-type electric force field for the explicit simulations of electrochemical CO dimerization on Cu (111) surface. *Chem Phys* **568**, 111821.
53. Li C-Y, Le J-B, Wang Y-H, Chen S, Yang Z-L, Li J-F, Cheng J, Tian Z-Q (2019) *In situ* probing electrified interfacial water structures at atomically flat surfaces. *Nat Mater* **18**, 697–701.
54. Kresse G, Furthmüller J (1996) Efficient iterative schemes for ab initio total-energy calculations using a plane-wave basis set. *Phys Rev B* **54**, 11169–11186.
55. Blöchl PE (1994) Projector augmented-wave method. *Phys Rev B* **50**, 17953–17979.
56. Grimme S, Ehrlich S, Goerigk L (2011) Effect of the damping function in dispersion corrected density functional theory. *J Comput Chem* **32**, 1456–1465.
57. Bi X, Yan Y, Wang H, Zhao Y, Zhang J, Wu M (2023) Electroreduction of $CO_2$ to $C_2H_4$ regulated by spacing effect: Mechanistic insights from DFT studies. *Energy Mater Adv* **4**, 0037.
58. Dattila F, Seemakurthi RR, Zhou Y, Lopez N (2022) Modeling operando electrochemical $CO_2$ reduction. *Chem Rev* **122**, 11085–11130.
59. Shao F, Wong JK, Low QH, Iannuzzi M, Li J, Lan J (2022) *In situ* spectroelectrochemical probing of CO redox landscape on copper single-crystal surfaces. *Proc Natl Acad Sci USA* **119**, e2118166119.
60. Li Z, Wang L, Wang T, Sun L, Yang W (2023) Steering the dynamics of reaction intermediates and catalyst surface during electrochemical pulsed $CO_2$ reduction for enhanced C2+ selectivity. *J Am Chem Soc* **145**, 20655–20664.
61. Nguyen TN, Chen Z, Zeraati AS, Shiran HS, Sadaf SM, Kibria MG, Sargent EH, Dinh CT (2022) Catalyst regeneration via chemical oxidation enables long-term electrochemical carbon dioxide reduction. *J Am Chem Soc* **144**, 13254–13265.
62. Lin SC, Chang CC, Chiu SY, Pai HT, Liao TY, Hsu CS, Chiang WH, Tsai MK, et al (2020) Operando time-resolved X-ray absorption spectroscopy reveals the chemical nature enabling highly selective CO(2) reduction. *Nat Commun* 11, 3525.
63. He M, Li C, Zhang H, Chang X, Chen JG, Goddard WA 3rd, Cheng MJ, Xu B, et al (2020) Oxygen induced promotion of electrochemical reduction of CO(2) via co-electrolysis. *Nat Commun* 11, 3844.
64. Mandal L, Yang KR, Motapothula MR, Ren D, Lobaccaro P, Patra A, Sherburne M, Batista VS, et al (2018) Investigating the role of copper oxide in electrochemical CO(2) reduction in real time. *ACS Appl Mater Interfaces* **10**, 8574–8584.
65. Qiao B, Wang A, Yang X, Allard LF, Jiang Z, Cui Y, Liu J, Li J, et al (2011) Single-atom catalysis of CO oxidation using Pt1/FeOx. *Nat Chem* **3**, 634–641.
66. Sikam P, Takahashi K, Roongcharoen T, Jitwatanasirikul T, Chitpakdee C, Faungnawakij K, Namuangruk S (2021) Effect of 3d-transition metals doped in ZnO monolayers on the $CO_2$ electrochemical reduction to valuable products: First principles study. *Appl Surf Sci* **550**, 149380.
67. Hu Y, Li Z, Li B, Yu C (2022) Recent progress of diatomic catalysts: General design fundamentals and diversified catalytic applications. *Small* **18**, 2203589.
68. Zhu L, Lin Y, Liu K, Cortés E, Li H, Hu J, Yamaguchi A, Liu X, et al (2021) Tuning the intermediate reaction barriers by a CuPd catalyst to improve the selectivity of $CO_2$ electroreduction to C2 products. *Chinese J Catal* **42**, 1500–1508.
69. Chen D, Chen Z, Lu Z, Tang J, Zhang X, Singh CV (2020) Computational screening of homo and hetero transition metal dimer catalysts for reduction of $CO_2$ to C2 products with high activity and low limiting potential. *J Mater Chem A* **8**, 21241–21254.
70. Roongcharoen T, Mano P, Jitwatanasirikul T, Sikam P, Butburee T, Takahashi K, Namuangruk S (2022) Theoretical insight on why N-vacancy promotes the selective $CO_2$ reduction to ethanol on NiMn doped graphitic

carbon nitride sheets. *Appl Surf Sci* **595**, 153527.
71. Mano P, Namuangruk S, Takahashi K (2023) Breaking BEP relationship with strong CO binding and low C—C coupling barriers for ethanol synthesis on boron-doped graphyne: Bond order conservation and flexible orbital hybridization. *J Phys Chem C* **127**, 7683–7694.
72. Dabsamut K, Takahashi K (2024) Controlling C—C coupling reactivity through pore shape engineering of B-doped graphyne family. *Carbon* **218**, 118672
73. Ou L, Long W, Chen Y, Jin J (2015) New reduction mechanism of CO dimer by hydrogenation to $C_2H_4$ on a Cu (100) surface: Theoretical insight into the kinetics of the elementary steps. *RSC Adv* **5**, 96281–96289.
74. Cheng T, Xiao H, Goddard WA 3rd (2015) Free-energy barriers and reaction mechanisms for the electrochemical reduction of CO on the Cu (100) surface, including multiple layers of explicit solvent at pH 0. *J Phys Chem Lett* **6**, 4767–4773.
75. Choi C, Kwon S, Cheng T, Xu M, Tieu P, Lee C, Cai J, Lee HM, et al (2020) Highly active and stable stepped Cu surface for enhanced electrochemical $CO_2$ reduction to $C_2H_4$. *Nat Catal* **3**, 804–812.
76. Luo W, Nie X, Janik MJ, Asthagiri A (2015) Facet dependence of $CO_2$ reduction paths on Cu electrodes. *ACS Catal* **6**, 219–229.
77. Sandberg RB, Montoya JH, Chan K, Nørskov JK (2016) CO—CO coupling on Cu facets: Coverage, strain and field effects. *Surf Sci* **654**, 56–62.
78. Wu ZZ, Zhang XL, Niu ZZ, Gao FY, Yang PP, Chi LP, Shi L, Wei WS, et al (2022) Identification of Cu (100)/Cu (111) interfaces as superior active sites for CO dimerization during CO(2) electroreduction. *J Am Chem Soc* **144**, 259–269.
79. Zhu C, Zhang Z, Zhong L, Hsu C-S, Xu X, Li Y, Zhao S, Chen S, et al (2021) Product-specific active site motifs of Cu for electrochemical $CO_2$ reduction. *Chem* **7**, 406–420.
80. Chang C-C, Ku M-S (2021) Role of high-index facet Cu (711) Surface in controlling the C2 selectivity for $CO_2$ reduction reaction: A DFT study. *J Phys Chem C* **125**, 10919–10925.